An experimental-numerical study of active cooling in wire arc additive manufacturing

An experimental-numerical study of active cooling in wire arc additive manufacturing

William Hackenhaar, José A. E. Mazzaferro, Filippo Montevecchi, Gianni Campatelli

PII: S1526612520300608

DOI: 10.1016/j.jmapro.2020.01.051

To appear in: *Journal of Manufacturing Processes*

Received Date: 14 October 2019

Revision Date: 9 January 2020

Accepted Date: 28 January 2020

Please cite this article as: Hackenhaar W, Mazzaferro JAE, Montevecchi F, Campatelli G. An experimental-numerical study of active cooling in wire arc additive manufacturing. Journal of Manufacturing Processes. 2020;52:58–65. https://doi.org/10.1016/j.jmapro.2020.01.051

Detailed Response to Reviewers

An experimental-numerical study of active cooling in wire arc additive manufacturing

William Hackenhaar[a], José A. E. Mazzaferro[a] , Filippo Montevecchi[b], Gianni Campatelli[b]

[a]Welding & Related Techniques Laboratory, Federal University of Rio Grande do Sul UFRGS/PROMEC, Porto Alegre, RS, Brazil
[b]*Department of Industrial Engineering, University of Firenze, Via di Santa Marta 3, Firenze, 50139, Italy*

Abstract

Wire arc additive manufacturing (WAAM) is a metal additive manufacturing process based on gas metal arc welding and it is known to be economically convenient for large metal parts with low complexity. The main issue WAAM is the sensibility to heat accumulation, i.e., a progressive increase in the internal energy of the workpiece due to the high heat input of the deposition process, that is responsible of excessive remelting of the lower layers and the related change in bead geometry. A promising technique to mitigate such issue is to use an air jet impinging on the deposited material to increase the rate of convective heat transfer. This paper presents an analysis of air jet impingement performances by means of a hybrid numerical-experimental approach. Different samples are manufactured using AWS ER70S-6 as filler material, using as cooling approaches free convection and air jet impingement, with different interlayer idle times. The measurement of substrate temperatures has been used to validate the process simulation, used for obtaining the temperature field of the whole part. The results indicate that air jet impingement has a significant impact on the process, limiting the progressive increase in the interlayer temperature as compared to free convection cooling. From the results arise that the optimal idle time is 30s, as a compromise between productivity and reduction of heat accumulation, independently from the cooling strategy.

Keywords: Wire arc additive manufacturing; Air jet impingement; Idle time

1. Introduction

Wire arc additive manufacturing (WAAM) is an additive manufacturing (AM) process that produces metal components through fusion and deposition of a metal wire using an electrical arc. Some advantages of WAAM compared to other metal AM processes are [1]: i) high deposition rate ii) possibility of manufacturing large parts iii) low capital investment iv) manufacturing efficiency, and v) possibility to rebuild damaged or worn parts. Considering standard welding process applied to WAAM, the rate of material deposition as indicated by Wu et al. [2] for Gas Metal Arc Welding (GMAW) standard transfer modes is about 3-4 kg/h, while for Cold Metal Transfer (CMT) about 2-3 kg/h. For processes that require the lateral wire feed as Gas Tungsten Arc Welding (GTAW) and Plasma Arc Welding (PAW) the deposition rates are respectively about 1-2 kg/h and 2-4 kg/h. An example of deposition rate calculated for a laser system is calculated by Xie et al. [3] for the alloy Ti-6Al-4V, and it accounts for about 500 g/h. However, these advantages are accompanied by a major drawback. In WAAM, the high heat input of the welding arc can lead to a progressive increase in the internal energy of the workpiece, known as heat accumulation [4], that could lead to excessive melting of the lower layers. This phenomenon occurs because the preferential cooling mode of the molten pool is heat conduction towards the substrate. Increasing the number of deposited layers decreases the magnitude of the conductive heat flux, causing the problem of heat accumulation. This phenomenon results in an increase in the molten pool size and interlayer temperature, i.e., the temperature of the top layer, at the start of the subsequent layer. Such effects result in a modification of the geometry of the layers [2,5] and the microstructure of the material [6,7] especially along the deposited height [8]. According to Wu et al. [2], in bimetal parts the deformation and residual stress are important due to the material difference in thermal expansion, where the interpass temperatures can play an important role to mitigate this issue.

A common way of preventing heat accumulation is to introduce interlayer idle times, i.e., allow the workpiece to cool down to a "safe" temperature before depositing the subsequent layer [9,10]. The drawback of this approach is that the idle times required to keep a constant interlayer temperature can be significantly high compared to the effective deposition time, resulting in a loss of productivity. An approach to decrease the interlayer idle times is to use active cooling systems to increase the heat transfer to environment, i.e., the convective heat transfer coefficient. Sasahara et al. [11] immersed the workpiece in a water cooled tank. Despite its effectiveness, the implementation of this system on existing welding facilities (e.g. welding robot cells), which is one of main advantages of WAAM, is impractical. Li et al. [12] used a thermoelectric cooling system based on the Peltier effect to cool the side surfaces of a vertical wall, i.e., a workpiece made of straight layers. The proposed solution provided a significant reduction of bead unevenness, grain size, and manufacturing time but its application to complex curved geometries is not straightforward. An alternative approach, easy to implement and suitable to manufacture complex parts, is to use a gas jet to increase the convective heat transfer coefficient. Wu et al. [13] used a CO_2 jet directed on the weld bead top surface by a nozzle attached to the welding torch. The system was tested by depositing a Ti6Al4V vertical wall test case, which showed an improvement in material strength, hardness, and manufacturing efficiency. A similar approach was also proposed by Montevecchi et al. [14], having two main differences with [13]: i) the usage of standard compressed air rather than CO_2, which can reduce the operational cost for materials less sensitive to the welding atmosphere than Ti6Al4V and ii) the target of the jet is not the top layer but the lower ones. This approach allows to have a larger surface for the impinging jet and results in a higher heat transfer [15]. A positive outcome of an effective air cooling during the deposition of subsequent layers, in which the electrical arc is not extinguished in starting and ending points, is to mitigate higher values and fluctuations of the residual stress in this location as indicated by Li et al. [16] in the deposition of circular layers using WAAM. Reddy et al. [17] proposed a technique based on the controlled cooling of the heated substrate, with the aim to obtain homogeneous properties along the vertical direction. The results of the tensile properties test in the Ti-6Al-4V alloy found by Wu et al. [18] points that it can be controlled by adjusting the heat input due to the mechanism of grain refinement. The potential effectiveness of the proposed method was assessed [14] using a validated model of jet impingement heat transfer coupled with a thermal model of the WAAM process. The results highlighted that jet impingement prevented an excessive increase of both molten pool size and interlayer temperature, making it a promising approach to prevent heat accumulation.

To increase the deposition rate Qi et al. [19] developed a solution that uses a double wire combination (7 mm wall thickness) that require an idle time of 60s for 2024 aluminum wire using free convection cooling. The resulting high thermal input required a following heat treatment and aging to enhance the mechanical properties of the part. The microstructure, fracture aspect and mechanical properties of the filler material AWS ER70S-6 deposited by WAAM was evaluated by Astarita et al. [20]. The study compared different orientations of the specimens respect to growth direction of the part using both tensile tests and microstructure analysis, that founded austenitic phase with small equiaxed grains in all the samples.

In the context of new strategies to hybrid-manufacturing, Ambrogio et al. [21] investigated the combination of additive manufacturing with traditional sheet forming process. A possible application is the local increase of the thickness of metal sheets by AM to reinforce the resistance or allow more complex parts. The use of laser metal wire deposition to produce thin walls was studied by Demir et al. [22]; this process has the advantage to allow the use of a large variety of alloy compositions and wire diameter. It was found a relation between the cooling rate and chemical composition with the mechanical properties of the produced part, enabling an increase of mechanical properties for Al-alloys adopting the correct setup. This process is an interesting alternative to WAAM when small features must be produced, also if it is characterized by a more complex path planning due to the lateral feeding of the wire.

Other direct metal deposition techniques, based on the use of laser and metal powder were investigated by Angelastro et al. [23]. An interesting application is also the hybrid electrical arc – laser approach proposed by Nasstrom et al. [24], where a trailing laser is added to a CMT torch to obtain topological improvements, and the study using a Finite Element Method for a laser drilling by Moradi et al. [25]. Specimens with lower build time, part weight and superior mechanical properties were generated by Moradi et al. [26] in a fused deposition modelling optimization study.

In this paper, a cooling system based on air jet impingement was implemented on a prototype WAAM machine. A test case workpiece was selected, and different samples were manufactured using free convection and jet impingement cooling. The filler material used in the deposits was the carbon steel AWS ER70S-6. The tests were carried out using different interlayer idle times to assess the performance of jet impingement cooling in different heat

accumulation conditions. The substrate temperature was measured at different points using K-type thermocouples. The temperature data acquired during the deposition of different samples were compared to assess the effect of air jet impingement on the substrate temperature. In order to evaluate the effect of air cooling on the interlayer temperature, the deposition of the samples was simulated using a Finite Element (FE) model. Simulation and thermocouple data were compared to evaluate accuracy of the model, that could be used to study the thermal history of any volume of the deposited part, allowing the study of phase transformation. The interlayer temperatures obtained by the simulation were used to compare the pattern of air jet and free convection cooling in the samples.

Nomenclature

A, B, C	Empirical factors to calculate jet impingement heat transfer coefficient
l	Nozzle to target surface standoff distance
Nu	Nusselt number, i.e. dimensionless heat transfer coefficient
Ø	Angular coordinate for jet impingement heat transfer coefficient calculation
r	Radial coordinate for jet impingement heat transfer coefficient calculation
d	Air nozzle diameter
Re	Reynolds number of the impinging air jet
α	Angle between the jet axis and the target surface
Δy	Nozzle offset along the *y* coordinate
Δz	Nozzle to torch offset along the *z* coordinate

2. Materials and methods

To evaluate the performance of the air jet impingement, this paper uses a hybrid numerical-experimental approach. Different samples of the test case were manufactured, and the substrate temperature was measured using K-type thermocouples. However, substrate-mounted thermocouples provide a limited insight into the heat transfer phenomena during deposition because they provide punctual data in a region far from the molten pool. To extend the investigation, an FE model was used to simulate the deposition of the test cases. Simulation results were then compared with the data obtained from the thermocouples to assess the accuracy of the model. Since the FE model returns the transient temperature field over the entire workpiece domain, an accurate prediction of the substrate temperature allows the heat transfer analysis to be extended to different regions. Therefore, the interlayer temperatures at the top of each layer were extracted from the simulation results, providing an important parameter to assess the effectiveness of jet impingement cooling. It must be pointed out that the presented analysis of the simulation results aims at providing a comparison of the interlayer temperature trends rather than accurately quantifying its punctual modifications.

Subsection 2.1 describes the experimental part of the work, i.e., the test case, the implementation of jet impingement cooling, and the conditions of the experiment. Subsection 2.2 depicts the FE model used to simulate the test case manufacturing.

1.1. *Experiments description*

This paper aims at assessing the effectiveness of air jet impingement in preventing heat accumulation of WAAM. The experimental test case is challenging geometry for heat accumulation: a vertical wall where its height is responsible for a reduction of the heat flux toward the substrate and the resulting heat accumulation. This value has been set to 50 mm was, adopting the test case geometry used by Wu et al. in [13], enough to have measurable effects of different cooling strategy and the idle time. The material used is the AWS ER70S-6 carbon steel, supplied as a 0.8 mm wire. In order to prevent excessive distortion, the substrate used was a 30 mm thick AISI 1040 block. The deposition was carried out using an AWELCO 250 Pulsemig GMAW power source connected to a retrofitted 3-axes milling machine. The combination of the process parameters was selected after some experimental tests to keep a stable arc with the lower possible heat input: arc voltage 18 V (constant voltage), current 93 A, wire feed speed 4.6 m/min, nozzle to workpiece distance 10 mm, travelling speed 200 mm/min, resulting in a heat input of 0.5 kJ/mm, and shielding gas Ar + 17% CO_2 supplied at 15 l/min. Such parameters resulted in welding beads that were 7.5 mm wide and 2.0 mm thick, requiring 25 layers to manufacture the selected geometry. It must be pointed out that the

accuracy of the FE modelling techniques used in this paper was previously verified with this set of process parameters [9], in order to have a reliable interlayer temperature analysis. The test case was positioned in the WAAM machine as shown in Fig. 1a. Fig. 2a depicts the orientation of the workpiece with respect to the axes of the WAAM machine.

The temperature of the substrate was monitored using 4 K-type thermocouples with a diameter of 1.29 mm. The thermocouples were non-shielded and had an exposed hot junction and ceramic insulation. The thermocouples were fixed to the top surface of the substrate, using spot welding, as shown in Fig. 1a. The positions of the thermocouples, with respect to the coordinate system, are marked in Fig. 2a. Using multiple measurement points allowed a more detailed comparison of the FE simulations and experiments. The data of the thermocouples were acquired using a National Instruments 9212 thermocouple module connected to a PC. All signals were recorded at a sampling rate of 10 Hz.

A coolant hose for machining applications with a 3 mm diameter nozzle was attached to the torch support. The low diameter of the nozzle was chosen to allow the positioning at different angles in the proximity of the welding torch. The hose was connected to 0.2 m^3 plenum and supplied with dry air at a pressure of 0.6 MPa. The air flow was initiated by a solenoid valve controlled by the numerical control of the WAAM machine in order to be synchronous with the deposition. The management of the valve was carried out thanks to a special macro of the numerical control specifically designed to enable an M function to control the solenoid that activates the impinging jet. Fig. 1a illustrates the implementation of the cooling system in the WAAM machine, while Fig. 1b shows the deposition of a sample, carried out using the proposed air jet cooling system.

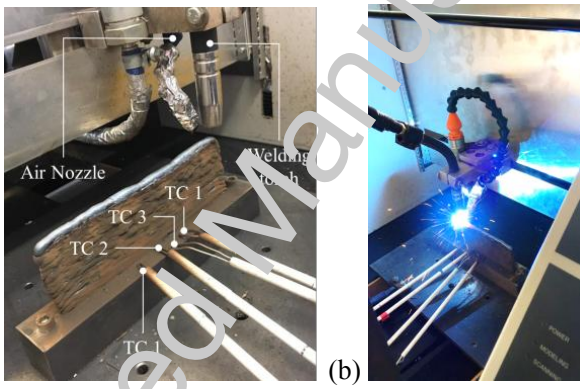

(a) (b)

Fig. 1. (a) Proposed cooling system, thermocouples arrangement and deposited test case. (b) Test case deposition using air jet cooling.

The selection of the jet parameters is important to achieve a high convective heat flux. According to Goldstein and Franchett [27], the local heat transfer coefficient of an air jet impinging on a target surface can be calculated using the correlation depicted in Eq. (1).

$$Nu(r,\phi) = A * Re^{0.7} exp\left(-\left(B + C\cos(\phi)\left(\frac{r}{d}\right)^{0.75}\right)\right) \quad (1)$$

Nu is the Nusselt number, i.e., the dimensionless form of the heat transfer coefficient, *Re* is the Reynolds number evaluated at the nozzle outlet section, *r* and ø define the polar coordinates of the target surface in a system centered at the intersection between the jet axis and the target surface, and *A*, *B*, and *C* are dimensionless coefficients determined by the experiments. Goldstein and Franchett [27] highlighted that such coefficient depends on the angle (α) between the jet axis and the target surface, and on the ratio (*l/d*) of the nozzle standoff distance and the nozzle diameter. Eq. (1) indicates that the heat transfer coefficient has an exponential decay from its maximum value at the intersection point. For decreasing α and increasing *l/d* values, *Nu* experiences an increase in the decay coefficient and in the peak value. Therefore, for a given nozzle diameter and air flow rate, a perpendicular jet and a low standoff distance increase the heat transfer coefficient. However, in WAAM, the increase of both α angle and nozzle proximity is limited by the interference of the air jet with the arc shielding gas, since excessive mixing can lead to arc instabilities, i.e., the disruption of the arc shielding gas region. Preliminary tests carried out with the nozzle perpendicular to the wall surface highlighted that this condition did not allow the achievement of a stable arc, irrespective of the air flow rate or the standoff distance. Based on these tests, the nozzle position and orientation

depicted in Fig. 2b with an inclination angle of 45° were adopted for the deposition tests. The geometry of the experimental test case is presented in Fig. 2b.

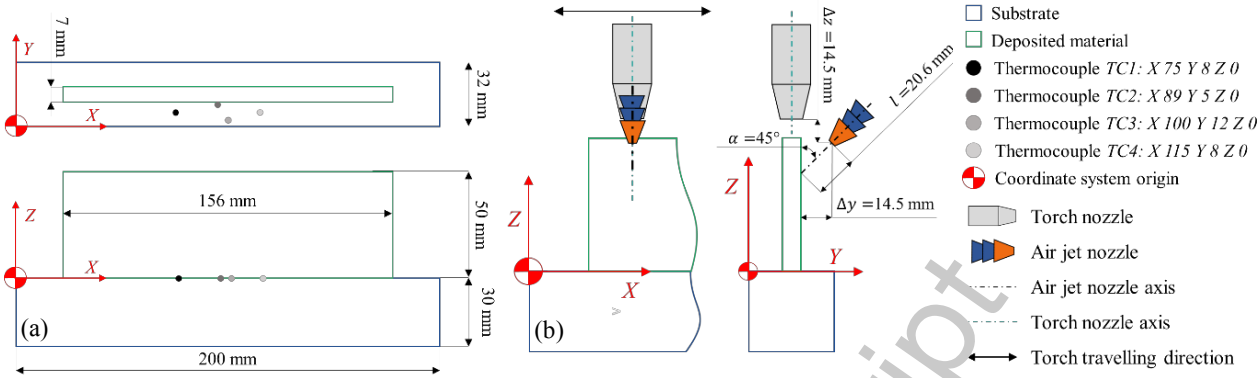

Fig. 2. (a) Test case geometry and thermocouple layout. (b) Air jet arrangement in the experiments.

The axis of the air nozzle was located in the same *XZ* plane as the axis of the torch, allowing the axis of the jet to intersect the wall surface at every *X* position of the torch, i.e., during the deposition of the entire layer. The offsets *Δz* and *Δy* (highlighted in Fig. 2b) define the position of the nozzle in the *YZ* plane. The offset *Δy* was set to the minimum possible value to avoid its interference with the substrate. In the case of *Δz*, decreasing its value moves the intersection of the axis of the jet and the target surface closer to the molten pool. This results in a higher fluid to surface temperature gradient, which increases the heat extraction. However, an excessive proximity to the border of the torch nozzle would result in an excessive contamination of the inert gas. Therefore, after many preliminary experimental tests, the value of 14.5 mm (Fig. 2b) was selected as a tradeoff between these opposite requirements. Based on an analysis of the Goldstein and Franchett correlation [27], the α angle was set to 45°, since lower angles resulted in a detrimental decrease of the heat transfer coefficients. Such a geometrical arrangement resulted in a distance, *l*, of 20.6 mm, i.e., in a *l/d* ratio of 6.9.

Further preliminary tests were carried out using the proposed jet orientation and location to identify the maximum achievable flow rate to prevent arc instability issues. *Re* of the selected flow rate was 22000, which is near to the center of the *Re* range covered by the Goldstein and Franchett [27] correlation.

As mentioned earlier, different samples of the test cases were manufactured using different idle times, in free convection and air jet cooling conditions. For all the samples, the first 10 layers were deposited using standard cooling and 120 s of interlayer idle time. This strategy was selected since activating the jet cooling below this level did not allow the air jet to target the wall surface. Idle time of 120 s was also used by Gou et al. [28] in the deposition of subsequent layers with Ti-6Al-4V using CMT process, allowing the deposited material cool down below the phase transition temperature. The interlayer idle time used by Li et al. [16] was 33 s and increment in the vertical direction of 1.6 mm in each layer. After layer number 10, the dimensions of the previous layers allowed the air to flow over the surface of the deposits, avoiding turbulence that could disrupt the shielding gas. Table 1 summarizes the conditions of each test, namely the idle times, cooling conditions, and the layer in which the air cooling is activated.

Table 1. Summary of manufactured test cases.

Test ID	Interlayer idle time [s]	Cooling condition	Initial jet cooling layer
1	120	Free convection	None
2	120	Jet impingement	14
3	30	Free convection	None
4	30	Jet impingement	11
5	10	Free convection	None
6	10	Jet impingement	11

1.2. *Finite element modelling*

The deposition process was simulated using a FE heat transfer analysis in order to obtain the full temperature field of the part, as similarly carried out by Casalino et al. [29], where FE simulation has used to predict the temperature profile in a laser surface transformation hardening with a cylindrical heat source of AISI 4130. The simulations were carried out using the commercial FE solver, LS-DYNA. The WAAM modelling techniques, such as the moving heat source, the elements activation algorithm, and the material behavior models, are based on previous research [30,31]. Fig. 3 shows the FE model used to simulate the deposition of the test cases.

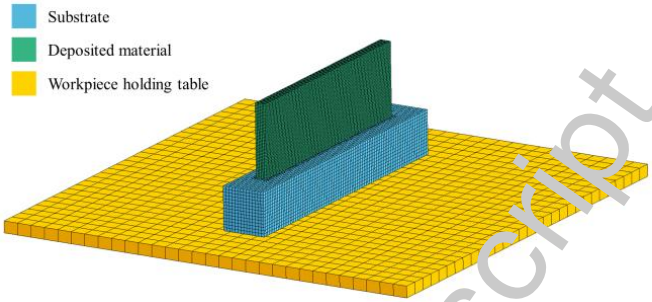

Fig. 3. FE model of the test case.

The geometry was discretized using 60274 1st order solid hexahedral elements, resulting in 75017 nodes. The modelling domain was extended to the mild steel workpiece holding table since the conductive heat flux from the substrate is a relevant contribution to the overall heat extraction. The conduction between the substrate and the workpiece holding table was included using a contact algorithm. The interface conductance was set to 2000 W/m^2°C based on literature data [32]. The effect of the air jet impingement was included using the technique presented in [14]. The different idle times were simulated by varying the length of the heat source on-off intervals. A 3D semi-elliptical moving heat source was used by Mirkoohi et al. [33] to predict the temperature profile in laser-based metal additive manufacturing, the authors also used thermal material properties as temperature dependent. In addition, it was found that the time spacing (time delay between two irradiations of the melt pool) does not have an influence on the evolution of thermal material properties.

3. **Results and discussion**

This section discusses the results of the hybrid numerical-experimental investigation on the effectiveness of air jet impingement. None of the manufactured samples showed evidence of any visible discontinuities. Subsection 3.1 presents the experimental results, discussing the overall trends of the thermocouples in the different tested conditions. Subsection 3.2 presents the comparison between the thermocouples and the simulation data, extending the comparison between air jet impingement and free convection cooling to the interlayer temperature pattern.

1.3. *Thermocouple results*

This section discusses the results of the substrate temperature measurements. As mentioned earlier, an initial set of layers was deposited using an interlayer idle time of 120 s. The value was then reduced according to Table 1. This section reports the results of the thermocouple TC2, since it was the closer to the deposited material, similar trends have been found for the other thermocouples. Fig. 4a shows the results of experiments 1, 3, and 5, related to the depositions carried out without air jet cooling. The experiments with air jet cooling were performed using the same idle times schemes used in the experiments without cooling. As mentioned in section 2, the first ten layers were deposited with 120 s of interlayer idle time and no cooling for all tests. Fig. 4b compares the results of the experiments using air jet cooling, namely tests 2, 4, and 6. It is highlighted that in the test carried out using air jet impingement and 10 s idle time, the trendline of the temperature lies below 250 °C, far lower the value of the same test performed using free convection cooling. This is clearly highlighted by Fig. 5b, which compares the results of tests 5 and 6.

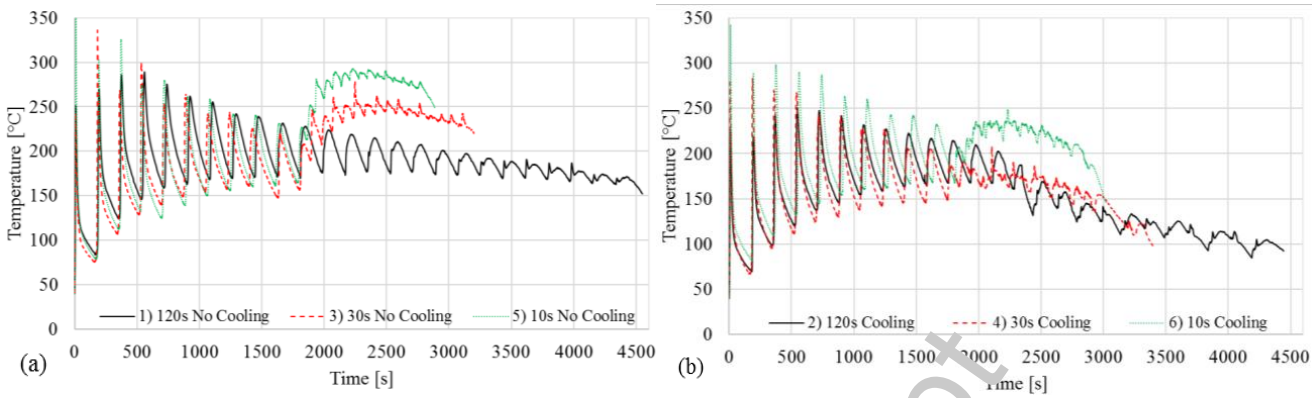

Fig. 4. (a) Deposited layers with no cooling. 1, 120 s. 3, 30 s. 5, 10 s. (b) Idle times for cooled deposits. 2, 120 s. 3, 30 s. 6, 10 s.

For all the tests, the temperature curves show a typical cyclic pattern, due to the repeated passes of the welding torch. However, the substrate temperatures show different patterns for different idle times. At its higher value, 120 s, the process shows a trend of a slight decrease in the temperature per each cycle, i.e., both peak and minimum values experience a progressive decrease. These results are in accordance with the effect of idle times in thermal cycles found by Lei et al. [10] and the decrease of the overall temperature as layers are deposited [34,35]. This behavior is due to the increase in the mass of the deposited metal and surface for each deposited layer, which respectively increase the overall heat capacity and the heat extraction by convection and radiation. Therefore, longer idle times allow these factors to dominate the heat transfer problem over the reduction of the conductive heat flux due to the increase of workpiece height. However, the adoption of longer idle times has the negative effect of decreasing the productivity. For this reason, lower idle times of 30 s and 10 s were tested, as shown in Fig. 4a. Both tests show a significant increase of the average temperature after the decrease of the idle times. This trend of substrate temperature is expected to result in a significant increase of the interlayer temperature in the top layers. These hotter regions can cause negative effects on the geometry of the layers, the surface quality, and the properties of the material.

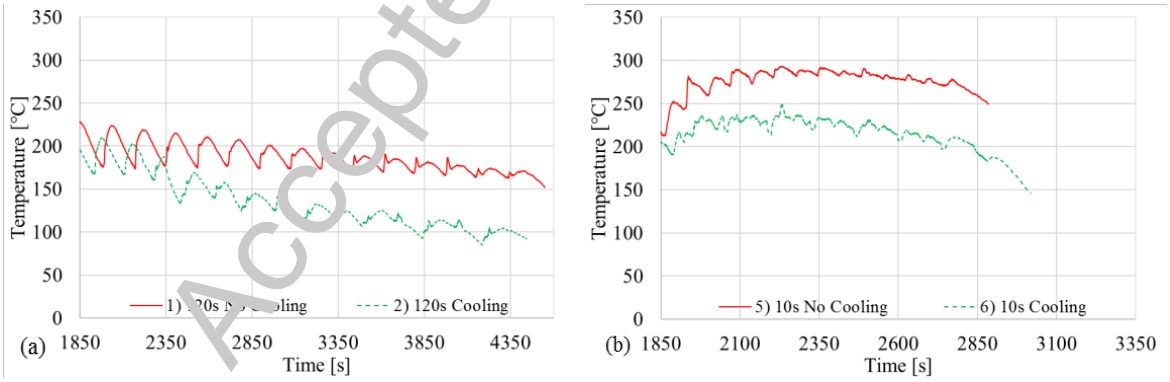

Fig. 5. Comparison of standard cooling and air jet cooling. (a) 120 s idle time. (b) 10 s idle time.

As shown in Fig. 5b, despite the use of air jet cooling, adopting an idle time of 10 s does not prevent the sudden increase in the substrate temperature. However, Fig. 5a, which compares the results with and without air cooling, using an idle time of 120 s, highlights that in this case the use of cooling results in a steeper decrease in the average substrate temperature. A similar trend occurs for an idle time of 30 s (Fig. 4b, test 4), where the substrate temperature experiences a significant reduction after the activation of the air impingement. Moreover, besides the similarities in the trends, tests 2 and 4 show close, punctual values after the activation of the air jet. This is an interesting result since, unlike in the free convection cooling tests, when using jet impingement, increasing the interlayer idle time above 30 s does not result in any significant reduction of the substrate temperature. Therefore,

increasing the idle time would only result in a loss of manufacturing efficiency. For the specific test case, reducing the idle time from 120 to 30 s would reduce the inactive period of the process for the layers produced with jet cooling by 75%. Considering that jet impingement is performed using compressed air, the increase of the cost is far lower than the saving due to the increased productivity, resulting in a positive balance for an active cooling strategy. It is important to notice that compressed air could be used only for low reactive materials such as carbon steel, while for highly sensitive materials such as Ti6Al4V it is required the use on an inert gas for the impinging jet.

Regarding the idle time selection, as shown by the results of test 6, its value cannot be reduced to zero also if using jet impingement. A limit condition for the idle time exists for a given combination of process parameters, workpiece geometry and size, material and jet parameters. This highlights how the jet impingement is not able by itself to assure a heat extraction as high as required to avoid the issue of heat accumulation but a contribution of an idle time, also if reduced, is always needed.

1.4. *Finite element method simulation results*

This subsection shows the effect of air jet impingement cooling by analyzing the results of FE simulations. The presented results are related to the simulations of test 1 and 2, that use an interlayer idle time value of 120 s. Fig. 6 presents the comparison of the results of the simulations with thermocouples 2 (TC2) and 4 (TC4), since such thermocouples are the closest and the farthest from the wall, respectively. The comparison was carried out by extracting the temperature time history of the nodes located in the closest position to the thermocouples.

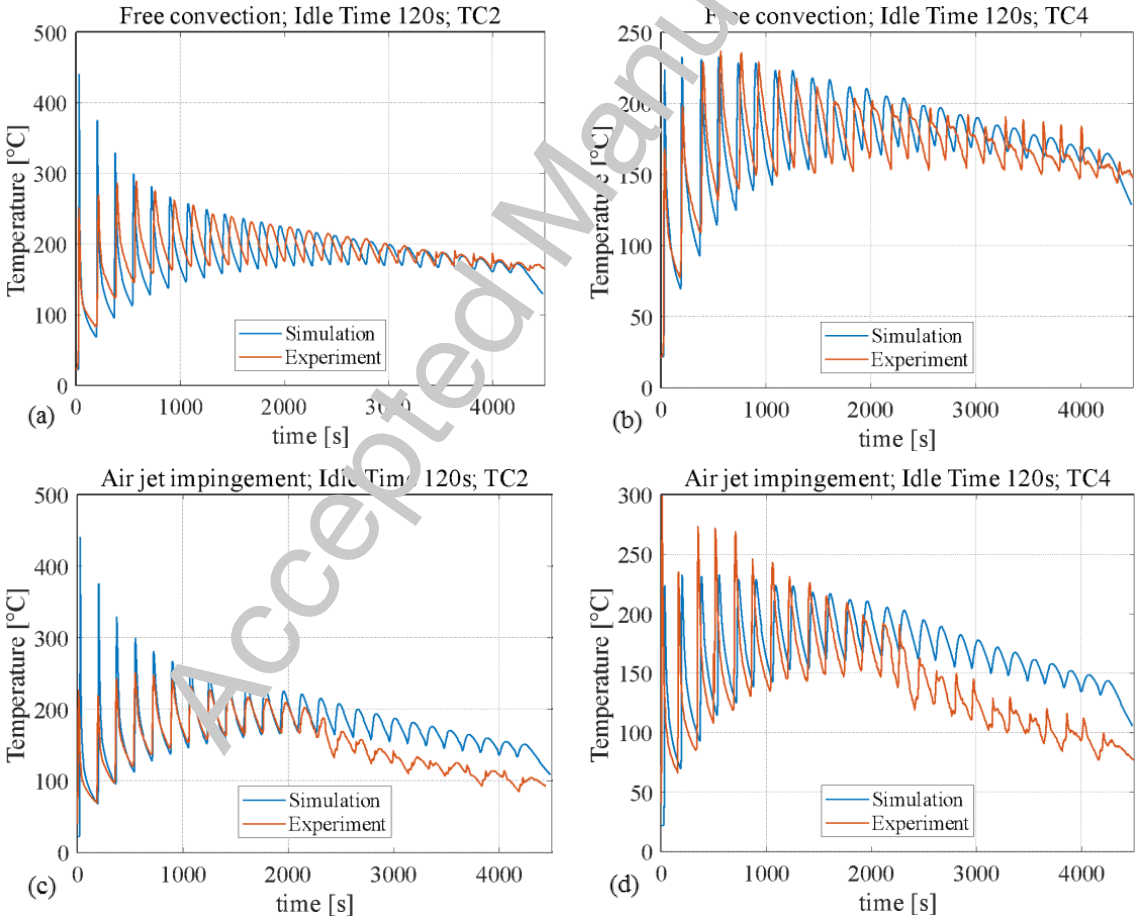

Fig. 6. Comparison of simulation and experimental results for 120 s idle time (a) TC 2, free convection cooling. (b) TC 4, free convection cooling. (c) TC 2 air jet impingement. (d) TC 4 air jet impingement.

Fig. 6a and Fig. 6b presents the data related to test 1, carried out in the free convection cooling condition. The comparison highlights a general agreement between the measured and simulated temperature patterns. The FE model is indeed capable of predicting the trend of both the minimum temperature per cycle and of peak to valley

amplitude. For TC2, the FE model overestimates the first temperature peaks. The reason for this overshoot could be related to the inherent uncertainties in the positioning of the thermocouples. This has a significant impact since TC2 is the closest to the molten pool and during the deposition of the first layer it is located in a steep temperature gradient area.

Fig. 6c and Fig. 6d present the results of the comparison for test 2, with air jet impingement. As in the case of test 1, the presented data highlights that the FE model predicts the overall trend of the temperature curves, including the effect of air jet impingement cooling. However, the FE model is not in perfect accordance with the experimental data with respect to the decrease rate of the average temperature per cycle after the activation of jet impingement. The reason for this could be an underestimation of the jet impingement heat transfer coefficients. The correlation of Goldstein and Franchett [27] was indeed developed studying air jets impinging on a smooth surface. The air jet impingement boundary condition includes only the target surface of the vertical wall. However, the air flow is also deflected on the top surface of the substrate, in which the convective heat transfer is modelled as free convection since it is difficult to quantify the correct heat transfer coefficient. This leads to a lower heat extraction than in the experiments. Moreover, WAAM workpieces have a slight surface waviness which could favor the flow turbulence and as a consequence, affect the heat transfer coefficients.

Although it is difficult to quantify the heat transfer coefficients precisely, the simulations showed a good agreement with the experimental data regarding the overall temperature trends, making them suitable for an analysis of the effect of air jet impingement on the interlayer temperature pattern. A set of control points was defined, located at the central point of the top surface of each deposited layer. For each control point, the first local minima in the temperature time history was considered as the interlayer temperature since it was the minimum temperature associated with the current control point after the deposition of the layer. Fig. 7 presents the results of the interlayer temperature comparison and the location of the control points for 120 s idle time.

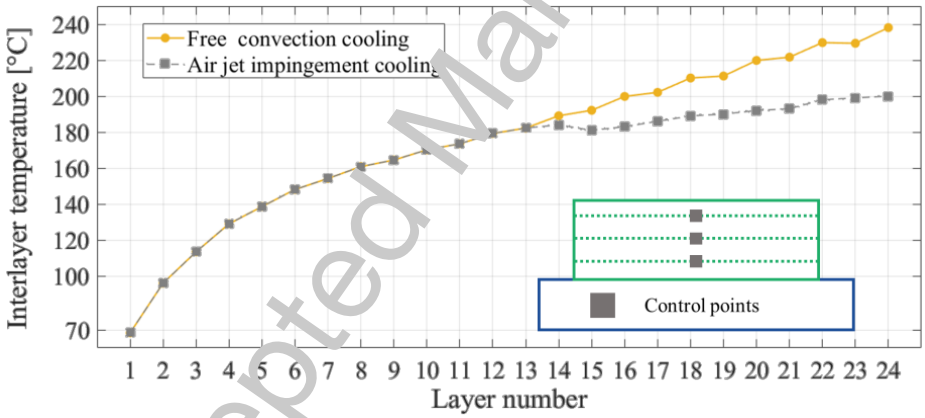

Fig. 7. Comparison of the simulated interlayer temperatures for free convection and air jet impingement cooling conditions.

In both curves the interlayer temperature increases throughout the deposition process. However, the curve related to the air jet impingement simulation shows a significant change in the curve slope after the activation of the air cooling. This confirms that the reduction of the substrate temperature observed in the thermocouple data indicates that jet impingement can limit the strong increase of the interlayer temperature. Moreover, considering the results presented in Fig. 6c and Fig. 6d, the jet impingement effect could be underestimated in the FE simulation. This could result in a further decrease of the slope of the interlayer temperature curve using air jet impingement. In agreement with [35], the potential of build-time savings and cost reduction due to inter-pass cooling were demonstrated in this work.

The main outlook of the presented research is to investigate the effect of air jet impingement on the properties and microstructure of materials sensitive to heat accumulation, such as Inconel 625. Different idle times and jet parameters should be tested to assess if, under specific conditions, jet impingement cooling could have a positive effect on the properties and microstructure of the deposited material. This optimization can be supported by the use of FE, to enable the selection of jet parameters and idle times to achieve a target interlayer temperature, for a given workpiece geometry, material, and process parameters.

4. Conclusions

This paper presents an analysis of the effectiveness of air jet impingement as a cost effective and versatile active cooling strategy to prevent heat accumulation in WAAM. A test case was manufactured using different interlayer idle times. Different samples were manufactured using both traditional free convection and air jet impingement cooling. The effectiveness of the jet impingement method was assessed using a hybrid numerical-experimental method, in which the measured substrate temperatures were compared to the FE simulation results. The validated simulation data were then used to extract the interlayer temperature during the deposition process.

The experimental data confirmed that the air jet impingement method reduced the substrate temperatures in all the tested configurations. In the tests conditions, when using air jet impingement, increasing the idle time from 30 s to 120 s did not result in a further decrease of the substrate temperature. However, the tests carried out using 10 s idle time highlighted that in this condition, the air jet impingement could not prevent an increase in the substrate temperature but could only reduce its magnitude. This suggests that, for a given process, workpiece size, and jet condition, there is a limit to the effectiveness of the air cooling.

The FE simulations accurately predicted the overall trend of the substrate temperature. The analysis of the results indicated that the decreasing trend of the substrate temperature resulted in a significantly slower increase of the interlayer temperature. This confirmed that air jet impingement can be an effective approach for controlling the interlayer temperature, without a significant increase in the idle times.

Acknowledgments

The author William Hackenhaar would like to acknowledge the support by the Brazilian research agency CAPES - PDSE [88881.189938/2018-01].

References

[1] Cunningham CR, Flynn JM, Shokrani A, Dhokia V, Newman ST. Invited review article: Strategies and processes for high quality wire arc additive manufacturing. Addit Manuf 2018;22:672–86. doi:10.1016/j.addma.2018.06.020.

[2] Wu B, Pan Z, Ding D, Cuiuri D, Li H, Xu J, et al. A review of the wire arc additive manufacturing of metals: properties, defects and quality improvement. J Manuf Process 2018;35:127–39. doi:10.1016/j.jmapro.2018.08.001.

[3] Xie R, Chen G, Zhao Y, Zhang S, Yan W, Lin X, et al. In-situ observation and numerical simulation on the transient strain and distortion prediction during additive manufacturing. J Manuf Process 2019;38:494–501. doi:10.1016/j.jmapro.2019.01.049.

[4] Wu B, Ding D, Pan Z, Cuiuri D, Li H, Han J, et al. Effects of heat accumulation on the arc characteristics and metal transfer behavior in Wire Arc Additive Manufacturing of Ti6Al4V. J Mater Process Technol 2017;250:304–12. doi:10.1016/j.jmatprotec.2017.07.037.

[5] Xiong J, Li Y, Li R, Yin Z. Influences of process parameters on surface roughness of multi-layer single-pass thin-walled parts in GMAW-based additive manufacturing. J Mater Process Technol 2018;252:128–36. doi:10.1016/j.jmatprotec.2017.09.020.

[6] Wu B, Pan Z, Ding D, Cuiuri D, Li H. Effects of heat accumulation on microstructure and mechanical properties of Ti6Al4V alloy deposited by wire arc additive manufacturing. Addit Manuf 2018;23:151–60. doi:10.1016/j.addma.2018.08.004.

[7] Wang JF, Sun QJ, Wang H, Liu JP, Feng JC. Effect of location on microstructure and mechanical properties of additive layer manufactured Inconel 625 using gas tungsten arc welding. Mater Sci Eng A 2016;676:395–405. doi:10.1016/j.msea.2016.09.015.

[8] Prado-Cerqueira JL, Diéguez JL, Camacho AM. Preliminary development of a Wire and Arc Additive Manufacturing system (WAAM). Procedia Manuf 2017;13:895–902. doi:10.1016/j.promfg.2017.09.154.

[9] Montevecchi F, Venturini G, Grossi N, Scippa A, Campatelli G. Idle time selection for wire-arc additive manufacturing: A finite element-based technique. Addit Manuf 2018;21:479–86. doi:10.1016/j.addma.2018.01.007.

[10] Lei Y, Xiong J, Li R. Effect of inter layer idle time on thermal behavior for multi-layer single-pass thin-walled parts in GMAW-based additive manufacturing. Int J Adv Manuf Technol 2018;96:1355–65.

doi:10.1007/s00170-018-1699-1.
[11] Takagi H, Abe T, Cui P, Sasahara H. Mechanical properties evaluation of metal components repaired by direct metal lamination. Key Eng Mater 2015;656–657:440–5. doi:10.4028/www.scientific.net/KEM.656-657.440.
[12] Li F, Chen S, Shi J, Zhao Y, Tian H. Thermoelectric cooling-aided bead geometry regulation in wire and arc-based additive manufacturing of thin-walled structures. Appl Sci 2018;8:207. doi:10.3390/app8020207.
[13] Wu B, Pan Z, Ding D, Cuiuri D, Li H, Fei Z. The effects of forced interpass cooling on the material properties of wire arc additively manufactured Ti6Al4V alloy. J Mater Process Technol 2018;258:97–105. doi:10.1016/j.jmatprotec.2018.03.024.
[14] Montevecchi F, Venturini G, Grossi N, Scippa A, Campatelli G. Heat accumulation prevention in Wire-Arc-Additive-Manufacturing using air jet impingement. Manuf Lett 2018;17:14–8. doi:10.1016/j.mfglet.2018.06.004.
[15] O'Donovan TS, Murray DB. Jet impingement heat transfer - Part I: Mean and root-mean-square heat transfer and velocity distributions. Int J Heat Mass Transf 2007;50:3291–301. doi:10.1016/j.ijheatmasstransfer.2007.01.044.
[16] Li R, Xiong J, Lei Y. Investigation on thermal stress evolution induced by wire and arc additive manufacturing for circular thin-walled parts. J Manuf Process 2019;40:59–67. doi:10.1016/j.jmapro.2019.03.006.
[17] Reddy S, Kumar M, Panchagnula JS, Parchuri PK, Kumar SS, Ito K, et al. A new approach for attaining uniform properties in build direction in additive manufactured components through coupled thermal-hardness model. J Manuf Process 2019;40:46–58. doi:10.1016/j.jmapro.2019.03.007.
[18] Wu Q, Ma Z, Chen G, Liu C, Ma D, Ma S. Obtaining fine microstructure and unsupported overhangs by low heat input pulse arc additive manufacturing. J Manuf Process 2017;27:198–206. doi:10.1016/j.jmapro.2017.05.004.
[19] Qi Z, Qi B, Cong B, Sun H, Zhao G, Ding J. Microstructure and mechanical properties of wire + arc additively manufactured 2024 aluminum alloy components: As-deposited and post heat-treated. J Manuf Process 2019;40:27–36. doi:10.1016/j.jmapro.2019.03.003.
[20] Astarita A, Campatelli G, Corigliano P, Epasto G. Microstructure and mechanical properties of specimens produced using the wire-arc additive manufacturing process 2019;0:1–11. doi:10.1177/0954406219883324.
[21] Ambrogio G, Gagliardi F, Muzzupappa M, Filice L. Additive-incremental forming hybrid manufacturing technique to improve customised part performance. J Manuf Process 2019;37:386–91. doi:10.1016/j.jmapro.2018.12.008.
[22] Demir AG, Biffi CA. Micro laser metal wire deposition of thin-walled Al alloy components: Process and material characterization. J Manuf Process 2019;37:362–9. doi:10.1016/j.jmapro.2018.11.017.
[23] Angelastro A, Campanelli SL, Casalino G. Statistical analysis and optimization of direct metal laser deposition of 227-F Colmonoy nickel alloy. Opt Laser Technol 2017;94:138–45. doi:10.1016/j.optlastec.2017.03.027.
[24] Näsström J, Brueckner F, Kaplan AFH. Laser enhancement of wire arc additive manufacturing. J Laser Appl 2019;31:022307. doi:10.2351/1.5096111.
[25] Moradi M, Golchin E. Investigation on the effects of process parameters on laser percussion drilling using finite element methodology; statistical modelling and optimization. Lat Am J Solids Struct 2017;14:464–84. doi:10.1590/1679-78253247.
[26] Moradi M, Meiabadi S, Kaplan A. 3D Printed Parts with Honeycomb Internal Pattern by Fused Deposition Modelling; Experimental Characterization and Production Optimization. Met Mater Int 2019;25:1312–25. doi:10.1007/s12540-019-00272-9.
[27] Goldstein RJ, Franchett ME. Heat transfer from a flat surface to an oblique impinging jet. J Heat Transfer 1988;110:84–90. doi:10.1115/1.3250477.
[28] Gou J, Shen J, Hu S, Tian Y, Liang Y. Microstructure and mechanical properties of as-built and heat-treated Ti-6Al-4V alloy prepared by cold metal transfer additive manufacturing. J Manuf Process 2019;42:41–50. doi:10.1016/j.jmapro.2019.04.012.
[29] Casalino G, Moradi M, Moghadam MK, Khorram A, Perulli P. Experimental and numerical study of AISI 4130 steel surface hardening by pulsed Nd:YAG laser. Materials (Basel) 2019;12. doi:10.3390/ma12193136.
[30] Montevecchi F, Venturini G, Scippa A, Campatelli G. Finite Element Modelling of Wire-arc-additive-

manufacturing Process. Procedia CIRP 2016;55:109–14. doi:10.1016/j.procir.2016.08.024.
[31] Montevecchi F, Venturini G, Grossi N, Scippa A, Campatelli G. Finite Element mesh coarsening for effective distortion prediction in Wire Arc Additive Manufacturing. Addit Manuf 2017;18:145–55. doi:10.1016/j.addma.2017.10.010.
[32] Sridhar MR, Yovanovich MM. Thermal contact conductance of tool steel and comparison with model. Int J Heat Mass Transf 1996;39:831–9. doi:10.1016/0017-9310(95)00141-7.
[33] Mirkoohi E, Sievers DE, Garmestani H, Chiang K, Liang SY. Three-dimensional semi-elliptical modeling of melt pool geometry considering hatch spacing and time spacing in metal additive manufacturing. J Manuf Process 2019;45:532–43. doi:10.1016/j.jmapro.2019.07.028.
[34] Lundbäck A, Lindgren LE. Modelling of metal deposition. Finite Elem Anal Des 2011;47:1169–77. doi:10.1016/j.finel.2011.05.005.
[35] Wu B, Pan Z, Chen G, Ding D, Yuan L, Cuiuri D, et al. Mitigation of thermal distortion in wire arc additively manufactured Ti6Al4V part using active interpass cooling. Sci Technol Weld Join 2019;24:484–94. doi:10.1080/13621718.2019.1580439.